

# Large Eddy Simulation of the Two-Phase Reactive Flow Field in a Single Sector Laboratory Scale Rich-Quench-Lean Combustion Chamber

D. Kaddar<sup>1</sup>, T. von Langenthal<sup>2</sup>, C. G. Weis<sup>\*2</sup>, F. C. C. Galeazzo<sup>3</sup>, P. Habisreuther<sup>2</sup>, N. Zarzalis<sup>2</sup>

<sup>1</sup> Institute for Simulation of reactive Thermo-Fluid Systems, TU Darmstadt, Otto-Berndt-Straße 2, Darmstadt 64287, Germany

<sup>2</sup> Engler-Bunte-Institute Division of Combustion Technology, Karlsruhe Institute of Technology (KIT), Engler-Bunte-Ring 7, 76131 Karlsruhe, Germany

<sup>3</sup>High Performance Computing Center Stuttgart (HLRS), Nobelstr. 19, 70569 Stuttgart, Germany

## Abstract

This work presents Large Eddy Simulation (LES) of a laboratory scale RQL combustion chamber. Simulations were carried out using an in-house LES-code for reactive, two-phase, adiabatic flow implemented in OpenFOAM. The two-phase turbulent reactive flow is modeled following a coupled Euler-Lagrange approach in combination with a presumed Joint Probability Density Function (JPDF) combustion model and tabulated chemistry. The reaction progress of laminar premixed flames is tabulated using a kerosene-surrogate chemical reaction mechanism. Calculated and measured velocity fields of the gaseous and liquid phase are compared to each other for reacting and non-reacting conditions. The results show excellent agreement between the two-dimensional flow fields derived from PIV and LES for the non-reactive case. The results of the reactive case show very good agreement for the velocity field.

## Introduction

RQL (Rich Burn / Quick Quench / Lean Burn) combustor configurations are common in modern aero engines due to their low NO<sub>x</sub> emissions and good flame stability [1]. The NO<sub>x</sub> formation in the fuel-rich primary zone is reduced due to the deficient availability of oxygen. Rapid admixing of secondary air with primary zone effluent is minimizing combustion zones with stoichiometric conditions and, ensuring oxidation of soot formed in the primary zone resulting in a minimum of soot emissions.

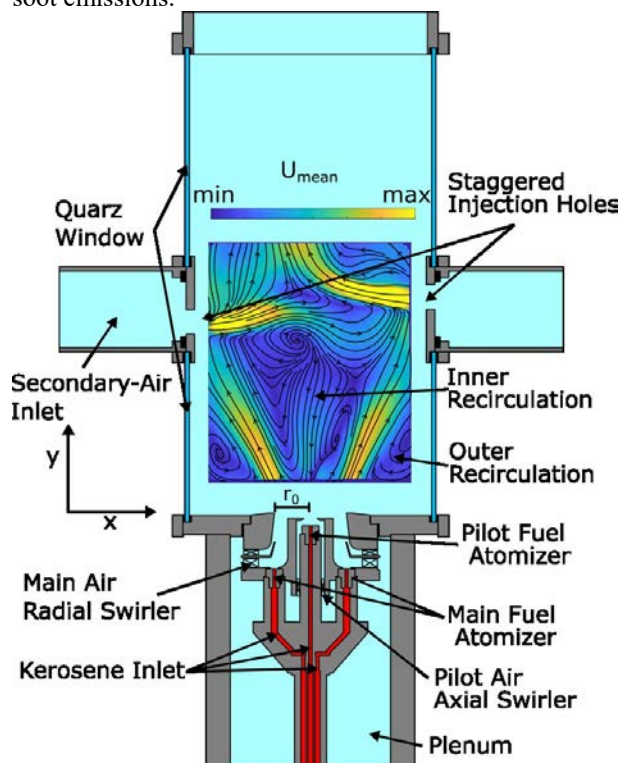


Figure 1: Single Sector Laboratory Scale Rich-Quench-Lean Combustion Chamber

In this context, experiments were carried out on an atmospheric, single sector combustion test rig, which is designed to be close to an aero-engine rich-quench-lean (RQL) combustor. The schematic cross-section sketch of the test rig is shown in Figure 1. The test rig features realistic pressure drop and inlet temperatures as well as overall dimensions. The combustion chamber has optical access through quartz glass windows from all sides and only the area of the secondary air injection is accessible via two sides. The secondary air injection consists of five holes per side in two rows in a staggered configuration. There is no window purging or external cooling in order to mitigate effects of cold walls.

The fuel nozzle consists of a pilot fuel atomizer, injecting kerosene fuel (Jet A-1) directly into the combustion chamber, and six main fuel atomizers, which inject the fuel directly after the main air swirler, allowing for some evaporation and mixing of the fuel before entering the combustion chamber. Main and pilot air have counter rotating swirl with swirl numbers of 0.7 and 1.34 respectively.

The combustion air is preheated to 600 K using electrical heaters and the pressure drop over the nozzle and secondary air injection is set to 3 %. The air fuel equivalence ratio in the primary zone is set to  $\phi = 1.43$ .

Figure 1 also shows a typical flow field of the combustor measured via Particle Image Velocimetry (PIV) [2]. The swirling flow creates a strong inner and outer recirculation zone and an unsymmetrical flow field due to the staggered mixing hole configuration. The injection of pilot fuel directly into the combustor creates a spray that is strongly visible in the PIV recordings.

In this study, the two-dimensional reactive and non-reactive flow fields derived from PIV are compared to numerical simulations. For the reactive flow field two simulations are carried out to determine the influence of the pilot fuel injection on the reactive flow field. The

injection of fuel into the combustor is modeled in two different ways. The fuel introduced by the main fuel atomizers is modeled as gas injection into the continuous phase, while injection of fuel by the pilot atomizer is modeled as a dispersed droplet phase. The simulations are carried out with and without pilot injection.

### Numerical Setup

The Software OpenFOAM version 5.0 [3] and a solver developed by the authors is used for Large Eddy Simulation (LES) of the non-reactive and reactive flow field inside the RQL-combustor. The Wall-Adapting Local Eddy-viscosity (WALE) model is employed for unresolved sub-grid scales [4] applying a turbulent Schmidt or Prandtl number of 0.85 if required. The filter width is calculated based on the cube root cell volume according to Deardorff [5]. On wall boundaries a wall function [6] accounting for the unresolved wall boundary layer is applied. Low-dissipation, second-order accurate central differencing / upwind blending scheme is applied for momentum- [7] (blending factor 0.2) and bounded second-order normalized variable diagram scheme for scalar discretization [8]. The Crank-Nicolson method is implicit, second-order accurate for time discretization [9].

Favre filtered transport equations are solved for density momentum, absolute enthalpy, mixture fraction [10] and unscaled reaction progress variable in accordance with Galleazzo et al. [11]. The progress variable is defined as the sum of complete combustion product mass fractions of water and carbon dioxide. The subgrid-scale variances are directly calculated via an algebraic approach [12,13].

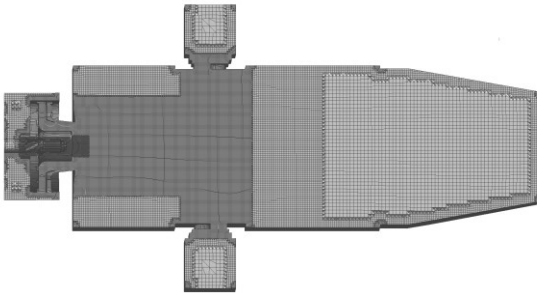


Figure 2: Cross section of numerical grid

Figure 2 shows a cross section of the numerical grid. The grid consists of 6.6 million cell at 3 refinement levels. The characteristic length of the unrefined cells is 2.5 mm, second level cells are 0.625 mm and the finest cells are 0.322 mm.

The source term of the reaction progress variable transport equation, thermodynamic data and species mole fractions are read from a lookup table. The lookup table is generated in a pre-processing procedure prior to the LES, by the calculation of one-dimensional premixed laminar stationary adiabatic flames for 33 different mixture fractions covering the range from lean to fuel-rich initial conditions. The method bases on the same principles as the Flamelet Generated Manifolds (FGM) method [14]. The initial temperature for the manifold generation equals the air inlet temperature of 600 K used

in the experiment. The laminar flamelets are calculated using a detailed chemical reaction mechanism for a kerosene surrogate consisting of 80 % n-decane (DEC) and 20 % 1,2,4-trimethyl-benzene (TMB) by weight [15]. The mechanism consists of 119 species and 522 reactions and has been validated against experimental data [16]. For each mixture fraction the solution is stored for 201 discrete points in normalized progress variable space. To account for the interaction between chemistry and turbulence a beta-pdf is used to calculate the joint probability parametrized by mean and variance values of a distribution. From a numerical multidimensional integration procedure [17], a table is derived which stores mean values of the various variables in the four dimensions of mean- mixture fraction and progress variable as well as their normalized variances. Eleven discrete values are used, in a linear distribution for the variance of the progress variable and in a logarithmic distribution for the variance of the mixture fraction. During LES, these four control variables are calculated and corresponding tabulated values are determined via multi-dimensional interpolation [18].

The source term in the transport equation for the mixture fraction is closed from Lagrangian Particle tracking for parcels of a dispersed kerosene phase. The Lagrangian dispersed phase is coupled with the Eulerian gas phase, besides the mass source term for the mixture fraction [19], via source terms in the momentum and total enthalpy transport equation [20][21]. The liquid phase is modeled as an ideal solution of DEC and TMB by a NRSDS [22] function assuring consistency with the surrogate formulation in the gas phase. As the lookup table is created only from adiabatic calculations, the decrease in enthalpy from the two-way coupling of the Eulerian with the Lagrangian phase is neglected.

During the Lagrangian parcel transport sub models are used to describe the thermo-physical phenomena within the parcels. Secondary breakup is modeled according to [23], where two breakup mechanisms are distinguished by characteristic Weber-number [24]. Evaporation and boiling are modeled [25] incorporating also the effect of flash evaporation. Turbulent drag is modeled depending on the local Reynolds-number [26]. Heat and mass transfer is modeled based on Sherwood number correlations [27] and a correction factor for Stefan flow [28].

The parcels are introduced at the position of the Pilot fuel atomizer. Inlet temperature and mass flow equal to the values for the operating conditions in the experiment. Injection pressure and spray angle are provided by the manufacturer of the atomizer. The parcels represent ensembles of droplets with corresponding droplet sizes in a Rosin-Rammler distribution. The Rosin-Rammler distribution bases on the Rosin-Rammler diameter and a shape parameter [29]. The shape parameter was chosen to be 3.5 corresponding to the arithmetic average value for the type of atomizer according to Levebre et al. [29]. The Rosin-Rammler diameter is derived from an empirical correlation for the characteristic Sauter mean diameter specific for the specific type of atomizer used in

the experiment[30]. The magnitude of the inlet velocity is calculated from an empirical correlation based on pressure drop and atomizer geometry [29].

### Velocity Field

The results from LES of the non-reactive flow field are averaged values of approx. 400.000 time steps covering 0.1 s of simulated time. Averaging was started after a minimum simulation time of ten turnover times, defined as the ratio of the domain volume divided by the overall volume flow at the outlet boundary. The averaged simulation time corresponds to approx. 2.4 turnover times.

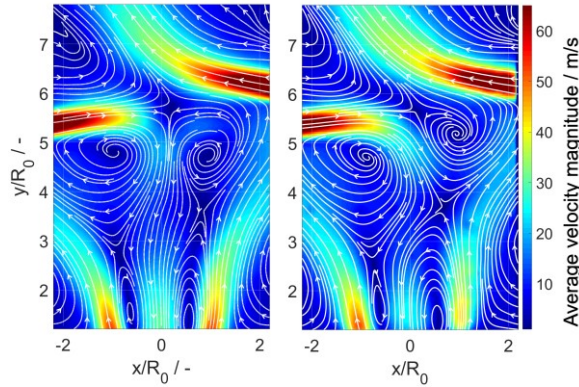


Figure 3: Contour plots of mean velocity magnitude in m/s for the non-reactive flow field from LES (left) and to PIV (right)

Figure 3 shows contour plots of the mean magnitude of the velocity from LES (left) and PIV (right) and corresponding streamlines. Both axes are the spatial coordinates (x; y) normalized with the nozzle radius (R0). From streamlines minor discrepancies in the shape of the inner recirculation zone can be identified. Concerning the contour plots, the air velocity magnitude of the main air flow at  $x/R_0 > 0$  is overestimated by the numerical simulation.

Detailed analysis of the flow field near the nozzle is shown by line plots of axial and radial velocity at three different heights above burner (HAB) in Figure 4. Minor discrepancies are observed for the radial velocity. Noticeable deviation between LES and PIV for axial velocity exists for the recirculation zone at  $HAB = 5$  mm, characterized by lower velocity at  $x/R_0 = 0$  in LES. Concerning radial velocity

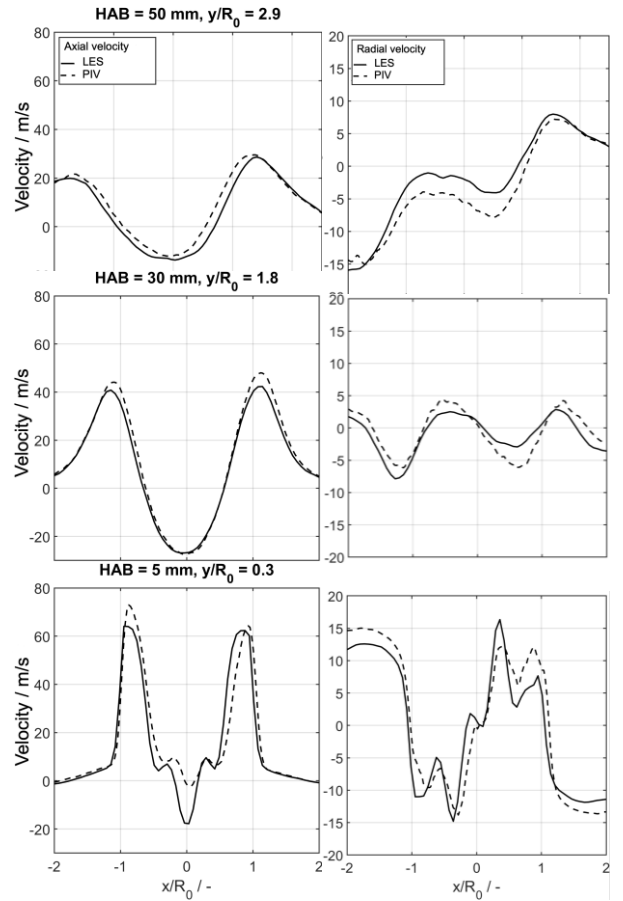


Figure 4: Line plots of axial (left) and radial (right) velocity in m/s over normalized radius at different heights above burner (HAB) in the non-reactive flow field

The averaging methodology for the reactive flow field simulation without pilot fuel injection is similar to the non-reactive case. For approx. 2.2 turnover times, 0.09 s of simulated times, the average of 330.000 time steps are calculated.

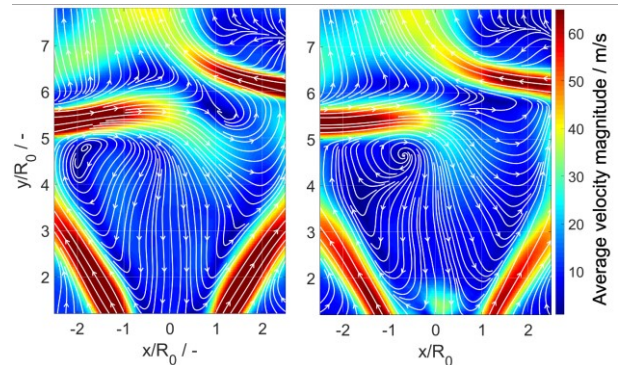


Figure 5: Contour plots of mean velocity magnitude in m/s for the reactive flow field without pilot injection from LES (left) and PIV (right)

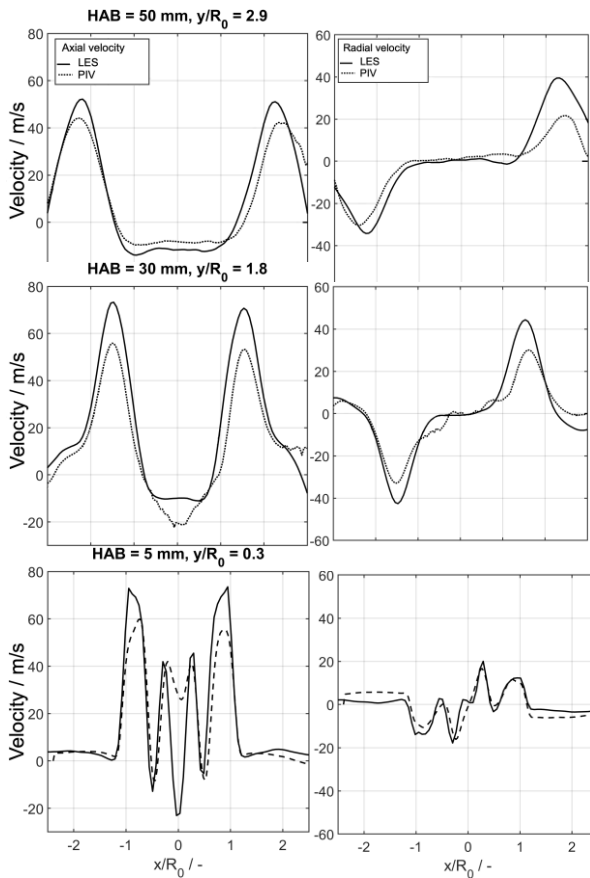


Figure 6: Line plots of axial (left) and radial (right) velocity in m/s over normalized radius at different heights above burner (HAB) in the reactive flow field, LES without pilot injection

Figure 5 shows contour plots of mean velocity magnitude and corresponding streamlines for the reactive flow field without pilot injection in LES. In contrast to Figure 3, the overpredicted velocity magnitude of the main inlets is significant in general. Furthermore, the penetration depth of the left secondary air injection jet is higher. Close to the nozzle, in the center area, the velocity magnitude is underpredicted by LES.

Line plots in Figure 6 confirm the general observations from Figure 4. Axial and radial velocity are overpredicted by LES. Similar to Figure 3, the recirculation zone very close to the nozzle only exists in LES. The results from two-phase LES with pilot injection do not differ significantly from LES without pilot injection as shown in the Appendix (Figure 8; Figure 9).

Concerning the two-phase flow, the instantaneous parcel distribution in two different areas, each with a dimension of 2 mm in HAB, and their velocity is shown in Figure 7. The variation of the parcel distribution with increasing HAB indicates an appropriate description of the spray angle.

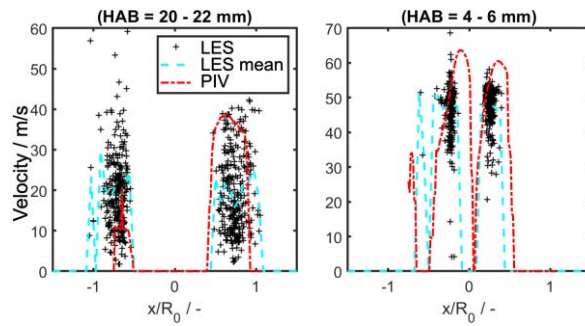


Figure 7: Instantaneous parcels (black cross) and mean velocity (light blue dashed line) from LES and mean velocity from PIV (red dashed-dotted line)

The spatial and velocity distribution of the injected parcels does not vary significantly from PIV. There is a clear indication that the methodology for the determination of the parcel injection resulted in a reasonable correct evolution of droplet transport in the primary zone.

### Conclusions

Calculated and measured velocity fields of the gaseous and liquid phase are compared to each other for different reacting and non-reacting conditions. The results show excellent agreement between the two-dimensional flow fields derived from PIV and LES for the non-reactive case. The results of the reactive case show very good agreement for the flow field. No significant influence of the pilot injection on the flow field is observed. Reasonable results for droplet spatial distribution and velocity in very good agreement with PIV are reproduced.

Strong evidence exists, indicating the applicability of the combustion model as well as the underlying methodology for the simulation setup of coupled Euler-Lagrange two-phase LES in the field of staged, stratified and highly turbulent combustion of kerosene with air.

### Acknowledgements

The authors gratefully acknowledge funding from the European Union within the SOPRANO H2020 project under Grant Agreement No. 690724.

### References

- [1] L. Smith, H. Karim, S. Etemad, W.C. and Pfefferle, The Gas Turbine Handbook, 2006.
- [2] T. von Langenthal, N. Zarzalis, M. Konle, in: Proceedings of the ASME Turbo Expo: Turbomachinery Technical Conference and Exposition - 2019: Presented at the ASME Turbo Expo 2019: Turbomachinery Technical Conference and Exposition, June 17-21, 2019, Phoenix, Arizona, USA, The American Society of Mechanical Engineers, New York, N.Y., 2019.
- [3] The OpenFOAM Foundation, OpenFOAM v5 User Guide, <https://cfd.direct/openfoam/user-guide>.
- [4] F. Ducros, F. Nicoud, T. Poinso, Wall-Adapting Local Eddy-Viscosity Models for Simulations in Complex Geometries, 1998.

- [5] J.W. Deardorff, The Use of Subgrid Transport Equations in a Three-Dimensional Model of Atmospheric Turbulence, *Journal of Fluids Engineering* 95 (1973) 429–438.
- [6] D.B. Spalding, A Single Formula for the “Law of the Wall”, *Journal of Applied Mechanics* 28 (1961) 455–458.
- [7] H.G. Weller, G. Tabor, H. Jasak, C. Fureby, A tensorial approach to computational continuum mechanics using object-oriented techniques, *Comput. Phys.* 12 (1998) 620.
- [8] H. Jasak, H.G. Weller, A.D. Gosman, High resolution NVD differencing scheme for arbitrarily unstructured meshes, *Int. J. Numer. Meth. Fluids* 31 (1999) 431–449.
- [9] J. Crank, P. Nicolson, A practical method for numerical evaluation of solutions of partial differential equations of the heat-conduction type, *Math. Proc. Camb. Phil. Soc.* 43 (1947) 50–67.
- [10] R.W. Bilger, The structure of turbulent nonpremixed flames, *Symposium (International) on Combustion* 22 (1989) 475–488.
- [11] F.C.C. Galeazzo, N.K. Fukumasu, J.A. Denev, C. Weis, P. Habisreuther, G.C. Krieger Filho, Change in Flame Geometry of an Ethanol Spray Flame by Varying the Spray Characteristics, *Combust. Sci. Technol.* 191 (2019) 1693–1710.
- [12] C.D. Pierce, P. Moin, A dynamic model for subgrid-scale variance and dissipation rate of a conserved scalar, *Physics of Fluids* 10 (1998) 3041–3044.
- [13] C.D. Pierce, P. Moin, Progress-variable approach for large-eddy simulation of non-premixed turbulent combustion, *J. Fluid Mech.* 504 (2004) 73–97.
- [14] J.A. van Oijen, L. de Goey, Modelling of Premixed Laminar Flames using Flamelet-Generated Manifolds, *Combust. Sci. Technol.* 161 (2000) 113–137.
- [15] S. Honnet, K. Seshadri, U. Niemann, N. Peters, A surrogate fuel for kerosene, *Proceedings of the Combustion Institute* 32 (2009) 485–492.
- [16] V. Vukadinovic, P. Habisreuther, N. Zarzalis, Influence of pressure and temperature on laminar burning velocity and Markstein number of kerosene Jet A-1: Experimental and numerical study, *Fuel* 111 (2013) 401–410.
- [17] F. Liu, H. Guo, G.J. Smallwood, Ö. Gülder, M.D. Matovic, A robust and accurate algorithm of the  $\beta$ -pdf integration and its application to turbulent methane–air diffusion combustion in a gas turbine combustor simulator, *International Journal of Thermal Sciences* 41 (2002) 763–772.
- [18] M. Kern, Modellierung kinetisch kontrollierter, turbulenter Flammen für Magerbrennkonzeppte, *Zugl.: Karlsruher Institut für Technologie, KIT, Diss., 2013, KIT Scientific Publ, Karlsruhe, Baden, 2013.*
- [19] B. Abramzon, W.A. Sirignano, Droplet vaporization model for spray combustion calculations, *International Journal of Heat and Mass Transfer* 32 (1989) 1605–1618.
- [20] C. Prathap, F.C.C. Galeazzo, P. Kasabov, P. Habisreuther, N. Zarzalis, C. Beck, W. Krebs, B. Wegner, Analysis of NOX Formation in an Axially Staged Combustion System at Elevated Pressure Conditions, *J. Eng. Gas Turbines Power* 134 (2012), doi:10.1115/1.4004720.
- [21] F. Eiberger, P. Habisreuther, N. Zarzalis, F. Turrini, in: *Volume 5C: Heat Transfer, American Society of Mechanical Engineers*, 06152015.
- [22] T.E. Daubert, R.P. Danner, *Data Compilation Tables of properties of pure compounds*, Am. Inst. of Chem. Engineers, New York, 1985.
- [23] R.D. REITZ, R. Diwakar, in: *SAE Technical Paper Series*, SAE International400 Commonwealth Drive, Warrendale, PA, United States, 1987.
- [24] M. Pilch, C.A. Erdman, Use of breakup time data and velocity history data to predict the maximum size of stable fragments for acceleration-induced breakup of a liquid drop, *International Journal of Multiphase Flow* 13 (1987) 741–757.
- [25] B. Zuo, A.M. Gomes, C.J. Rutland, Modelling superheated fuel sprays and vaproization, *International Journal of Engine Research* 1 (2000) 321–336.
- [26] G.L. Hubbard, V.E. Denny, A.F. Mills, Droplet evaporation: Effects of transients and variable properties, *International Journal of Heat and Mass Transfer* 18 (1975) 1003–1008.
- [27] W. Ranz, W. Marshall, *Evaporation from Drops*, *Chemical Engineering Progress* (1952) 141–146.
- [28] R.B. Bird, W.E. Stewart, E.N. Lightfoot, *Transport phenomena*, 2nd ed., Wiley, New York, 2007.
- [29] A.H. Lefebvre, V.G. McDonell, *Atomization and sprays*, CRC Press, Boca Raton, London, New York, 2017.
- [30] X.F. Wang, A.H. Lefebvre, Mean drop sizes from pressure-swirl nozzles, *Journal of Propulsion and Power* 3 (1987) 11–18.

## Appendix

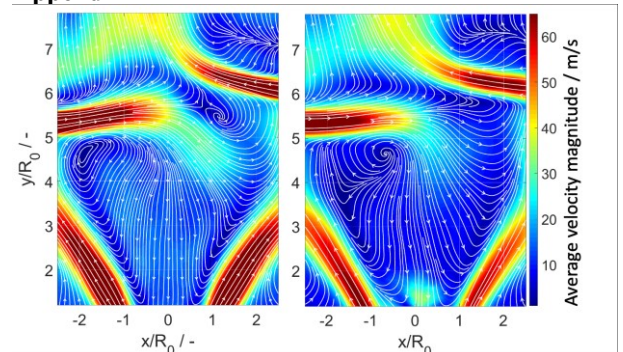


Figure 8: Contour plots of mean velocity magnitude in m/s for the reactive flow field with pilot injection from LES (left) and PIV (right)

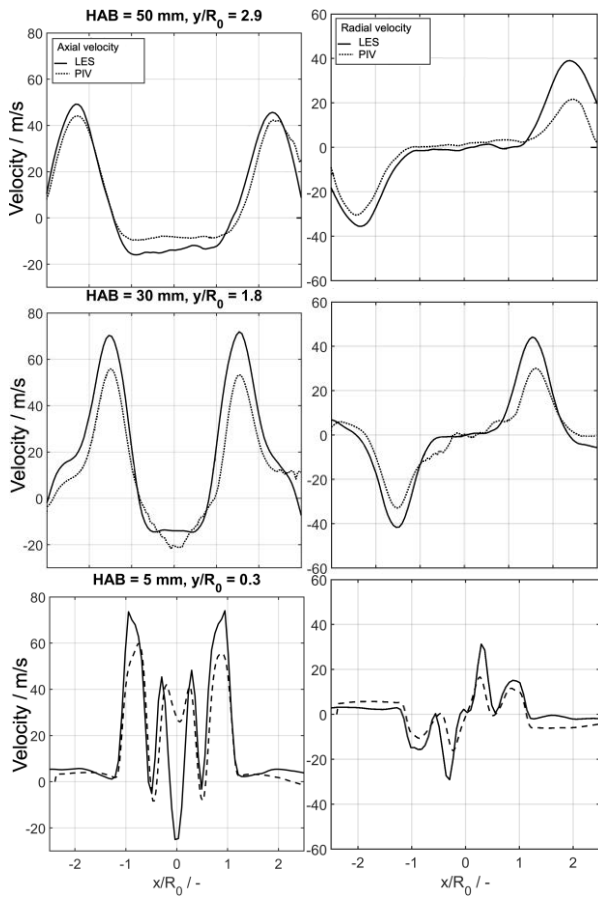


Figure 9: Line plots of axial (left) and radial (right) velocity in m/s over normalized radius at different heights above burner (HAB) in the reactive flow field, LES with pilot injection

## Repository KITopen

Dies ist ein Postprint/begutachtetes Manuskript.

Empfohlene Zitierung:

Kaddar, D.; Langenthal, T. von; Weis, C. G.; Galeazzo, F. C. C.; Habisreuther, P.; Zarzalis, N.  
[Large Eddy Simulation of the Two-Phase Reactive Flow Field in a Single Sector Laboratory Scale Rich-Quench-Lean Combustion Chamber](#)  
2021. 10th European Combustion Meeting (ECM 2021), April 14-15, 2021, Virtual Edition. Proceedings Volume, 1121–1126, MCM  
[doi:10.5445/IR/1000146401](https://doi.org/10.5445/IR/1000146401)

Zitierung der Originalveröffentlichung:

Kaddar, D.; Langenthal, T. von; Weis, C. G.; Galeazzo, F. C. C.; Habisreuther, P.; Zarzalis, N.  
[Large Eddy Simulation of the Two-Phase Reactive Flow Field in a Single Sector Laboratory Scale Rich-Quench-Lean Combustion Chamber](#)  
2021. 10th European Combustion Meeting (ECM 2021), April 14-15, 2021, Virtual Edition. Proceedings Volume, 1121–1126, MCM

Lizenzinformationen: [KITopen-Lizenz](#)